Neurobiology of Disease 130 (2019) 104523

Contents lists available at ScienceDirect

Neurobiology of Disease

journal homepage: www.elsevier.com/locate/ynbdi

Predicting disease specific spinal motor neurons and glia in sporadic ALS

Fabien Dachet[a], Jiangou Liu[a], John Ravits[b,*], Fei Song[a,*]

[a] Department of Neurology and Rehabilitation, University of Illinois at Chicago, Chicago, IL 60612, USA
[b] ALS Translational Research Program, Department of Neurosciences, University of California, San Diego, CA 92093, USA

A B S T R A C T

Increasing evidence shows that neuroinflammation mediated by activated glia and infiltrated immune cells is involved in the pathogenesis of sporadic amyotrophic lateral sclerosis (sALS). However, the mechanisms of interaction between activated glia and motor neuron degeneration are unclear. To determine the relationship between motor neurons and glial activation in the central nervous system of sALS patients, we applied new cellular interactome bioinformatics tools to transcriptome profiles established from laser captured motor neurons in regions remote from site of onset. We found a disease specific subtype of motor neuron that inversely correlated with survival of sALS patients. Interestingly, two subtypes of motor neurons (motorneuron2 and 3) and two subtypes of microglia/macrophages (microglia/macrophage1 and 2) were unique to sALS patients compared to controls. Increased microglia/macrophage1 correlated with decreased motorneuron2 and increased microglia/macrophage2 correlated with decreased motor neuron3. Increased MHC class II genes correlated with microglia/macrophage1–2. Tissue staining using immunofluorescence confirmed a significant increase of microglia/macrophage expressing MHC class II, suggesting that they were activated. Identified gene pathways and biological changes included apoptosis and protein phosphorylation in motorneuron3 and antigen processing/presentation and immune cell activation in microglia/macrophages in sALS patients. Our findings support the hypothesis that neuro-glia physical interactions are important in pathogenesis, and targeting disease-specific motor neurons and/or glia could be a useful therapy to slow disease progression.

1. Introduction

Amyotrophic lateral sclerosis (ALS) is a fatal, adult-onset neurodegenerative disorder that affects motor neurons in the brain and spinal cord (Rowland and Shneider, 2001). Unlike familial ALS, 95% of ALS is sporadic (sALS) with no known genetic component (Byrne et al., 2011). Motor phenotypes of sALS suggest that underlying motor neuron degeneration begins focally in the neuraxis and progresses contiguously outward along neuronal anatomy (Ravits and Spada, 2009). It has been proposed that a spiraling cascade mediated by immune and/or inflammatory signals between neurons and glia may underlie the temporal and spatial propagation. Neuroinflammation has long been known to be a key component of ALS pathology (Boillee et al., 2006) (Turner et al., 2004), and microglial activation has been implicated in mediating the neuropathology of SOD1 G93A transgenic mice (Frakes et al., 2014). The interactions between motor neurons and glia and the roles of inflammation and immunity in ALS are both complex. The central nervous system (CNS) contains its own intrinsic immune cells, primarily microglia, that act as the monocytes/macrophages of the CNS (Perry et al., 2010) (Sargsyan et al., 2005). Both activated microglia and macrophages are important in initiating immune responses. *Activated microglia and macrophages express major* histocompatibility complex (*MHC*) *class II proteins that are normally found on antigen-presenting cells.* In humans, the MHC class II protein complex is encoded by the human leukocyte antigen gene complex (HLA). Experiments using SOD1 animal models have demonstrated that the ALS phenotype is dependent on disease-related gene expression in both neurons and glia, thus supporting both cell autonomous and non-cell autonomous mechanisms of disease (Boillee et al., 2006) (Graber et al., 2010) (Henkel et al., 2009) (Ilieva et al., 2009) (Yamanaka et al., 2008). In addition to glia, T-cells have been shown to play a role in modulating neuron degeneration in sALS, with T-helper/regulatory cells possibly determining the degree of microglial activation and associated disease progression (Appel et al., 2010) (Appel, 2009) (Beers et al., 2008).

The clinical -pathological observation in sALS patients shows that maximal areas of spinal motor neuron loss correlate with the site of disease onset, suggesting that the location and spread of motor neuron degeneration in sALS patients begins in one region and works its way to adjacent regions of the spinal cord (Ravits et al., 2007a) (Ravits et al., 2007b). As the spinal motor neuron loss advances from rostral to caudal regions in patients with bulbar and arm onset disease, respiratory failure intervenes before lumbar regions are fully advanced, thus providing an opportunity for studying motor neurons that are at risk but still existing at less affected regions of the spinal cord. We previously assayed alterations in exon splicing and gene expression in RNA pools separately from laser captured motor neurons and their surrounding anterior horns using exon microarray analysis (Rabin et al., 2010). In the present study, we utilize a novel bioinformatics approach (Dachet

* Corresponding authors.
E-mail addresses: jravits@ucsd.edu (J. Ravits), feisong@uic.edu (F. Song).

https://doi.org/10.1016/j.nbd.2019.104523
Received 17 April 2019; Received in revised form 19 June 2019; Accepted 1 July 2019
Available online 02 July 2019
0969-9961/

et al., 2015) to re-analyze the transcriptome sets and understand the proximate microenvironment associated with sALS pathogenesis.

2. Materials and methods

2.1. Clinical-pathological-genomic data

All nervous systems were acquired by way of an Investigational Review Board and Health Insurance Portability and Accountability Act compliant process (Rabin et al., 2010). The acquisition and de-identification of postmortem tissues was approved either by Benaroya Research Institute (2003 − 2011) or University of California San Diego's (after 2011) IRB in accordance with relevant guidelines and regulations. Subsequent use of de-identified postmortem tissues was in accordance with standard federal guidelines and regulations and is not considered Human Subjects research. The generation of transcriptome profiles has been previously reported (Rabin et al., 2010). All tissues were acquired using an Investigational Review Board and Health Insurance Portability and Accountability Act compliant process. We studied 12 sALS samples and 10 control samples - patient demographics are re-stated for convenience (Supplemental Table 1). The lumbar spinal cords were from patients with bulbar or arm onset sALS and control nervous systems were from patients in the hospital's critical care unit when life support was withdrawn. Autopsies were performed within 6 h of death and both frozen and formalin-fixed paraffin-embedded (FFPE) tissue sets were created from alternating adjacent regions. We profiled gene expression in laser captured motor neurons using exon array technology. We used immunofluorescence for histopathological study.

3. Bioinformatics to detect differentially expressed genes and cellular interactome

The microarray analysis of ALS versus control samples was performed using GEO2R (NCBI, https://www.ncbi.nlm.nih.gov/geo/geo2r) with default parameters. The normalized expression of the differentially expressed probes was used to search for Pearson correlation profiles utilizing the same methods as previously described (Dachet et al., 2015). 5377 probes (representing 2938 unique genes) were found DE with a *p*-value less or equal to 0.005 between ALS samples and control samples. Expression values of these DE probes were clustered using Pearson correlation metric and visualized using Cytoscape V2.8.3 (Smoot et al., 2011). The composition of each cluster identified with the plugin Allegro Mcode (AllegroViva Corporation, 2011) was assigned a putative cell label using literature mining approaches. The profile of expression of each cluster was composed by averaging the normalized expression of all the probes forming the cluster. The relations between the profiles of expression of the clusters were visualized by hierarchical clustering using the 'R' library 'pvclust' with a Pearson correlation metric.

3.1. Confirmation of transcriptome results by histopathology

Tissue sections of lumbar spinal cord were cut transversely at 5 μm thickness, dewaxed, cleared with xylene, and hydrated through a graded series of alcohol solutions. The antigen retrieval was performed with 10 mM EDTA, pH 6.0, for double immunofluorescent stained microglia with MHC class II (HLA-DR alpha) or with citrate buffer, pH 6.0, for MHC class I (HLA-A, B, C). The sections were then washed three times in Tris-Buffered Sodium (TBS), pH 7.4, blocked using 5% normal goat serum for 1 h at room temperature, and incubated with primary antibodies overnight at 4 °C. Primary antibodies were used to identify microglia and astrocytes, including polycolonal Iba-1 (1:500, Cat. No.019–19,741, Wako, Richmond VA), monoclonal HLA-DR alpha (1:40, Cat. No. M0746, Dako Inc.), and polycolonal GFAP (1:500, Cat. No. Z0334, Dako Inc., Carpinteria, CA). The tissue slides were then incubated for 1 h with either goat anti-rabbit antibody tagged with Alex-488 or goat anti-mouse antibody tagged with Alex-549 (1:500, Jackson Immuno Inc. West Grove, PA), stained with red fluorescent Neuro Tracer (Nissl body) (1:300, Cat. No. N-21482, Molecular Probes. Eugene, OR), and mounted with mounting medium (Cat. No. H-1400, Vector Laboratories, Burlingame, CA). For MHC class I (HLA-A, B, C, 1:400, clone EMR8–5, Cat. No. Ab70328, Abcam, Cambridge, MA) and Iba1 double staining, the sections were incubated for 1 h with biotinylated goat anti-rabbit antibody (Cat. No. 111–065-003, 1:500, Jackson Immuno Inc. West Grove, PA) and goat anti-mouse antibody tagged Alex-647 (1:500, Jackson Immuno Inc. West Grove, PA), followed by streptavidin conjugated with Alexa Fluo-488 (Cat. No. 016-540-084, 1:500, Jackson Immuno Inc. West Grove, PA), and mounted with mount medium with Dapi (Cat. No. H-1200, Vector laboratories). The control slides were treated exactly the same as above, but with no primary antibodies.

3.2. Quantification of histopathology

The Digital images (20×) of whole lumbar spinal cord were obtained with a Leica DM5500B microscope fluorescence microscope (Leica Microsystems Inc., Wetzlar, Germany) and scanned automatically with the multiple channel option in a Q (Imaging) cooled CCD camera (SN: Q36526, Canada). The specific fluorescent labeled cellular markers surrounding each individual motor neuron in the laminae zone IIIV-IX in the ventral horn were analyzed using Metamorph Software 7.8 with colour channel separation.

The co-localization of microglia/macrophages (Iba1) and MHC class II (HLA-DR alpha) was quantified by the measure co-localization according to Metamorph's manual. The area of microglia/macrophages was measured as the function 'thresholded area' within 5 μm away from the edge of each motor neuron in the laminae zone VIII-IX of a ventral horn from the double stained spinal cord images (20×). The selected images were separated by two channels (green = Iba1 and red = MHC class II) using Display (colour separation), the thresholds were set for both channels, and co-localization was measured using the Apps. The data was presented as the percentage of co-localized area from sALS and control patients (n = 3 patients/each group).

The co-localization of microglia/macrophages (Iba1) and MHC class I (HLA-ABC) was quantified manually. The merged area of co-localized microglia/macrophages and MHC class I was measured as the function 'thresholded area' within 5 μm away from the edge of each motor neuron in the laminae zone VIII-IX of a ventral horn from the double stained spinal cord images (20×). The data was presented as the mean of co-localized objects per motor neuron from sALS and control patients (n = 3 patients/each group).

Similarly, to quantify astrocytes surrounding individual motor neurons, each motor neuron was defined using positive Nissl body staining with a clear nucleolus in the laminae zone IIIV-IX of each ventral horn. Astrocyte (GFAP positive) fluorescence was measured as the function 'thresholded area' within the region of 5 μm away from the edge of each motor neuron. The data was presented as a percentage of thresholded area from sALS and control patients (n = 3 patients/each group).

4. Results

4.1. Uniquely identified different subtypes of motor neurons and microglia/macrophages in sALS patients

We identified 2938 genes (15% of the total number of genes) that were differentially expressed (DE) at p-value ≤0.005 using R script (Dachet et al., 2015). These DE gene clusters showed highly consistent and exact inverse patterns when we compared 12 sALS samples versus 10 control samples (Fig. 1A). Eight clusters were separated using allegroMcode and the in silico analysis of the profiles of Pearson correlation

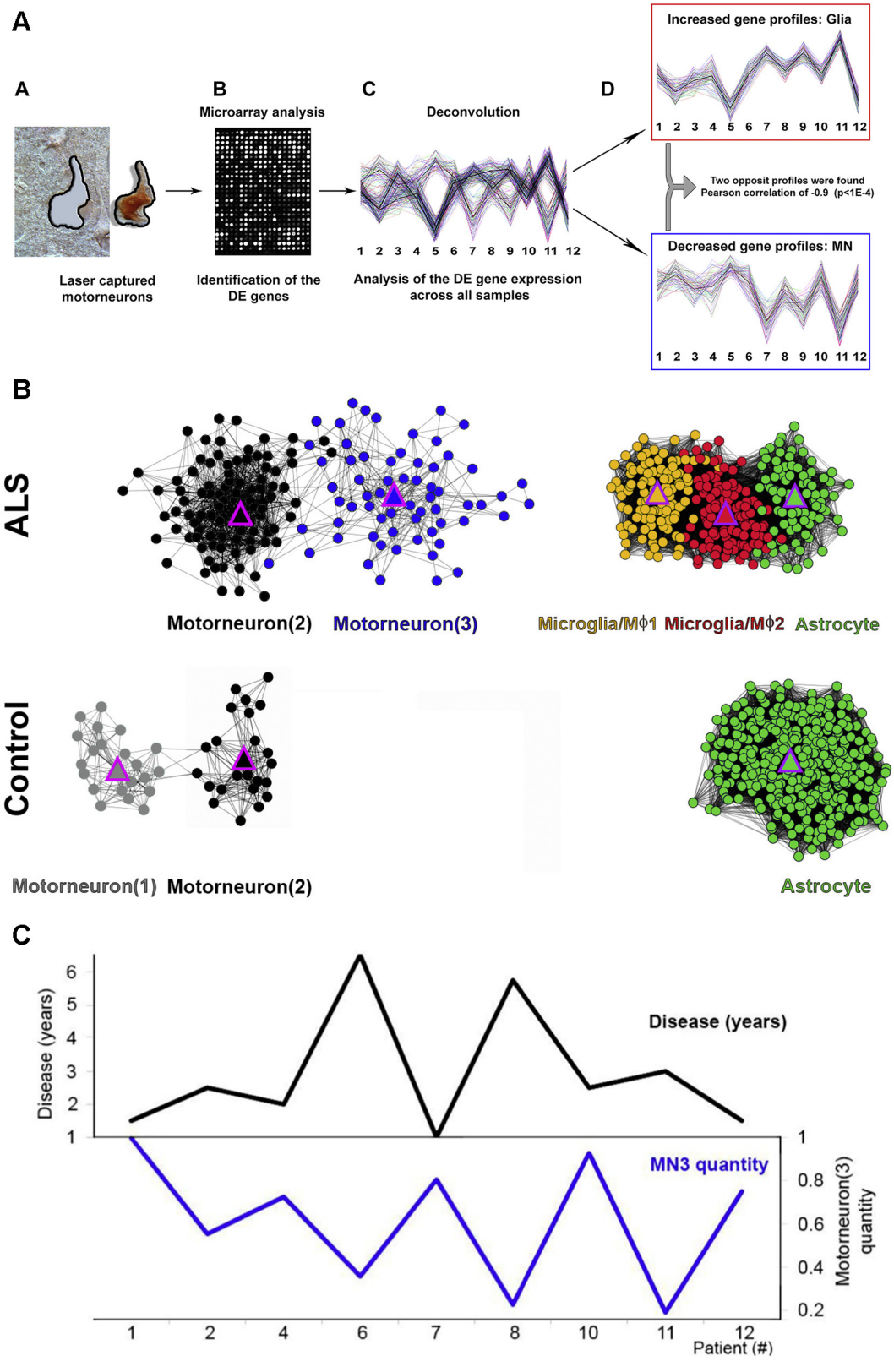

(caption on next page)

of the DE probes (Fig. 1B). We identified different subtypes of motor neurons (MN): subtypes one and two (MN1 and MN2) from control patients; and subtypes two and three (MN2 and MN3) from sALS patients (Fig. 1B). Based on our best knowledge, it is the first reported study to identify different subtypes of motor neurons using a cellular interactome in the less affected regions of spinal cords. It would help us understand the disease progression in sALS patients.

Interestingly, we found that all decreased gene profiles were motor neuron genes that exactly and inversely associated with all increased glial gene profiles within the captured motor neuron

Fig. 1. Differentially expressed gene clusters reveal cellular interactome showing both motor neurons and glia, and unique motorneuron3 in sALS patients negatively correlated with the disease course. (A) Special processing of spinal cord motor neuron collection and selective enrichment of relevant cellular compartments for genomic analysis. Laser capture microdissection permits collection and selective enrichment of lumbar motor neurons for genomic analysis (a). All motor neurons from each patient's ventral horns were pooled together for RNA extraction. Exon array hybridization was performed in all patients including 12 patients with sALS and 10 control patients (b). The differentially expressed (DE) gene across all patients was deconvoluted using 'R' scripts (c). The deconvolution shows two major expression profiles with an opposite relationship between glia and motor neurons (d). (B) Cell type specific patterns of differentially expressed gene clusters reveals cellular interactome showing both motor neurons and glia within the sampled areas. Spinal cord motor neurons at lumbar levels (less affected area) were collected by laser microdissection from sALS patients ($n = 12$) with bulbar/arm disease onset (more affected area) and control patients ($n = 10$) for genomic studies. Using our novel bioinformatics method, the differentially expressed (DE) genes were clustered by Pearson correlation ($r \geq 0.84$, $p < 0.01$) to build up a cellular interactome to predict changes in cellular composition. The DE genes were separated in 8 clusters: 3 clusters in controls and 5 clusters in sALS patients. Using literature mining algorithms and manual annotations, each cluster was identified as a cell type corresponding to a different colour. The pink triangle corresponds to the centroid of the cluster. (C) MN3 negatively correlated with survival. Survival time in 75% of sALS patients (9 out of 12, Supplemental Table 1) showed a negative correlation with the quantity of MN3 ($r = -0.73$, $p < 0.05$). (For interpretation of the references to colour in this figure legend, the reader is referred to the web version of this article.)

microenvironments in each patient. Using literature mining algorithms and manual annotations, we identified 8 specific cell types (Table 1, Fig. 1B).

List of gene in each in-silico assigned cell type. Each gene has been found differentially expressed in ALS samples at p value ≤ 0.005 and cluster of correlation with $r > 0.84$.

In sALS patients, we identified 5 cell types: two different subtypes of motoneurons (MN2 and MN3), two groups of microglia/macrophages (MG/Mϕ), and astrocytes. In control patients, we identified 3 cell types: two different subtypes of motoneurons (MN1 and MN2) and astrocytes. Compared to control patients, the subtype 3 motor neuron (MN3) and groups 1 and 2 MG/Mϕ were uniquely identified only in sALS patients. Taken together, these data suggest that captured motor neurons contain microenvironments closely surrounding glia that provide an activated 'natural' microenvironment where the interaction between MN connected glia occurs during disease progression in sALS patients. We next wanted to determine the nature of these unique connectomes and their relationship between the disease specific MNs and glia.

To understand the mechanism underlying why activated macrophages and microglia made their connections with 3 subtypes of MNs (MN1, MN2 and MN3) in the less affected regions, we looked at the affected biological process and gene pathway in control and sALS patients (Table 2). In sALS patients, we found metabotropic glutamate receptor process involvements in subtype 2 motor neurons (MN2), but immune cell activation and G-protein signaling process involvements in subtype 3 motor neurons (MN3). In glia, we found cell adhesion signaling and apoptosis involvements in astrocytes and MG/Mϕ1, but antigen presenting and T cell activation signaling involvements in MG/Mϕ2. The connection between macrophage/microglia and MN2/MN3 at the less affected areas suggests that these cellular and molecular signaling pathways could serve as therapeutic targets.

To investigate whether the different types of motor neurons relate to the disease progression, we analyzed the relationship between subtypes of motor neurons and survival time of sALS patients. We found that the survival time significantly correlated with decreased MN3 in 9 out of 12 sALS patients (Fig. 1C). However, MN2 did not show any correlation with patients' survival. The data implies that the MN3 could play an important role in patients' survival and serve as a potential biomarker and/or therapeutic target.

4.2. Activated MG/Mϕ1–2 connected with MN2–3 in sALS

Our hierarchical clustering of the profiles showed the interplay between different subtypes of motor neurons and glial cell types. The increased MG/Mϕ1 inversely associated with decreased MN2, while increased MG/Mϕ2 inversely associated with decreased MN3 in 12 ALS patients (Fig. 2A, $p < 0.05$). Increased HLA-DRA (MHC class II) genes positively correlated with MG/Mϕ1 and MG/Mϕ2 (Fig. 2B), suggesting that these microglia and macrophages, which very closely connect with MNs, were activated (Fig. 2B). The quantitation confirmed significantly increased activation of microglia/macrophages within the sampled areas in the ALS patients when compared to control patients using tissue staining with both MG/Mϕ and MHC class II (HLA-DRA) specific antibodies (Fig. 2C).

4.3. MN2 connected with reactive astrocytes in both sALS and control patients

Astrocytes have been known to be a component of human ALS pathology implicated in mediating the neuropathology of ALS (Ilieva et al., 2009) (Vargas and Johnson, 2010). The increased astrocytes inversely associated with decreased MN2 and MN3 in 12 ALS patients, but with decreased MN2 in 10 control patients, respectively (Fig. 3A). Increased HLA-DRA (MHC class II) genes positively correlated with astrocytes (Fig. 3A), suggesting that these astrocytes, which very closely connect with MN2, were activated in both control and sALS patients. Quantitation using both reactive astrocyte-specific antibody (GFAP) and Nissl substance for staining astrocytes and motor neurons confirmed no changes of reactive astrocytes within the sampled areas when comparing sALS to control patients (Fig. 3B).

4.4. MN2 inversely correlated with MHC class I expression in both sALS and control patients

MHC class I molecules present intracellular protein to cytotoxic T cells for the induction of cytotoxic T cell responses in ALS (Nardo et al., 2016). Increased MHC class I expression on microglia was shown in the brain and spinal cords in ALS tissues (Kawamata et al., 1992) (McGeer et al., 1993), suggesting the possible role of MHC class I in ALS pathology. We found that increased gene expression HLA-B (MHC class I) positively associated with MG/Mϕ1 in sALS patients but with astrocytes in control patients (Fig. 4A). However, MHC class I (HLA−B) expression negatively correlated with MN2 in both sALS and control patients (Fig. 4A). Through tissue staining using MHC class I (HLA-A,B,C) specific antibodies, we found that capillaries, normally acting as a positive control for MHC class I, were stained in both sALS and control tissues (data not shown). However, it was not detectable in motor neurons in both sALS and control patients (Fig. 4B). While microglia/Mϕ consistently increased in sALS patients (Fig. 4C), the colocalization of MHC class I expression and microglia/Mϕ showed no change between sALS and control patients (Fig. 4D).

4.5. Proposed model of different subtypes of motor neurons connected with different types of glia

We and others previously reported the activation of glia in ALS which (Ilieva et al., 2009) (Vargas and Johnson, 2010) (Song et al., 2012) (Song et al., 2014), in combination with our new findings in the particular microenvironment at less affected spinal cord regions, suggests a putative theory of motor neuron pathologic spread in sALS (Fig. 5). MN1 and MN2 were present in non-neurological disorder conditions. MN2 and MN3 were present in the less affected regions

Table 1
Gene lists for specific cell type.

MN1	MN2	MN3	MG/Mϕ1	MG/Mϕ2		Astrocyte
Down-regulated			Up-regulated			
BC008284	ABCA3	AKAP8L	A2M	ABCA8	TMEM123	ABCA1
BC131497	ADAM19	AP5S1	ABCB1	ADIPOR2	TOP2B	ABCC9
C15orf52	ADGRL1	AR	APOD	AEBP1	TREM2	AHCYL1
CACNA1D	AKT1S1	ATP13A2	C7	ALDH1A1	TRIP6	ALDH1A1
CBX2	AR	CALM1	CALCRL	ANTXR1	VCAM1	AQP4
CPD	BC034223	CCDC19	CASP8	ANXA1	VCAN	ASPA
DNTT	BC035744	CLCN6	CDCA7L	ASH1L	XRN1	C1orf61
GREB1L	BC125017	CLDN1	CFH	C4A	YAP1	C3
GRLF1	BRSK2	COL5A1	COBLL1	CCND2	YTHDC1	CD44
KRT77	CABP1	COL7A1	COL12A1	CD74	ZEB2	CD81
LTB4R2	CACNA1A	CTBS	COL1A2	CDC14A	ZHX2	CHPT1
MADD	CAMKMT	CYP26C1	COL6A3	CETN3		CNN3
MYBPC2	CDH17	DIS3L2	CXCR4	CHN2		CST3
OR4D9	CKAP2	DNAJB12	CYBRD1	CSRP1		CTNNA3
PRKCG	DEDD2	DSCR9	CYP1B1	CTNNA3		DTNA
PTPRN2	EFNA5	DZANK1	CYR61	CYBRD1		EFHD1
SAPS1	ELAVL3	ENTPD3	DCN	DDR2		ERBB2IP
SLC12A5	FAM135B	EPHB1	DSE	DHRS3		FAM107A
SUSD2	FGF11	FAM101A	EFEMP1	DST		FAM198B
TMEM128	FOXRED1	GATA5	FBLN1	EPB41L2		GATM
ZBTB7A	GIT1	GDF15	FN1	EPS8		GFAP
	GLRA3	KPTN	GSN	ERBB2IP		GPM6B
	GNAZ	L1CAM	GYPC	ETS1		GPR177
	GRIN2A	LINC00308	HDAC1	FAM198B		GTPBP1
	GRIN2B	LOC284352	IFI44	FYB		HSPA2
	GRLF1	LOC653319	ITGBL1	GIMAP4		IGSF6
	HECW1	LRSAM1	ITIH5	GJA1		KIF13B
	HUWE1	LTBP4	KCTD12	GMFG		NDRG2
	KIAA1409	MAP3K11	LAMA2	GOLIM4		NTRK2
	L1CAM	MC1R	LAMA4	GPR177		PLEKHB1
	MADD	MED16	LEF1	GRAMD3		PMP2
	MGC19604	MPL	LTBP1	GSTM5		PRKCA
	NELL2	MTNR1B	LTBP2	HERC5		PRTFDC1
	NPLOC4	NDUFAF3	MATN2	HLA-DPA1		PTGS1
	NRK	NEK5	MEF2C	HLA-DPB1		PTPRZ1
	NTRK2	NFATC1	NEDD9	HLA-DRA		QKI
	NUP93	NKX3–1	NFASC	JAM2		SEPT2
	PACSIN1	NR1H3	NOTCH2	KCTD12		SERPINE2
	PCBP3	PCNA	NR2F1	MARCKS		SLC16A9
	PFKP	PCSK4	PARP14	MOCS1		SLC40A1
	PI4KA	PSMD1	PDGFRA	MXI1		SSPN
	PKN1	PSMD7	PLXND1	MYO6		STON1
	PLEKHA6	PTCH2	PTBP1	NKTR		TDRD3
	PPP1R17	RAB40C	PTGDS	PCAF		TJP2
	PRDM4	RPS6KL1	PTN	PCDH18		VCAN
	PRUNE2	SAPS1	PTPN13	PRDM5		WWC1
	PSD3	SIN3B	TJP1	PRKD3		
	RNFT2	SLC22A1	TRIM38	PRKG1		
	SECTM1	SLC38A2	TXNIP	PTGDS		
	SLC35C1	SLC5A10	UTRN	PYHIN1		
	SPTB	TEX35	VIM	QKI		
	SUSD2	TNS1	VPS13C	RARRES3		
	TK2	TNS2	WWTR1	RBP1		
	TM7SF3	TPSD1		RFTN2		
	TMEM16D	TRPC6		ROBO3		
	TMEM59L	TTI2		RSRP1		
	TOM1L2	UBE2J2		SASH1		
	TRIP13	VPS37B		SEPP1		
	TSPAN33	WARS		SERBP1		
	TUBB3	WDFY4		SLC1A3		
	TUBG2	WDR90		SLC40A1		
	VPS13A	ZBTB7A		SLC7A2		
	VSTM2A			SPARC		
	ZNF606			SULT1C4		

under disease conditions. Unique cell types identified in early/progressive sALS were microglia/macrophages (MG/Mϕ1 and MG/Mϕ2) and MN3 (Fig. 2B). In control patients, reactive astrocytes expressing both MHC class I and II connected with MN2 (Fig. 3). In sALS patients, reactive astrocytes expressing MHC class II connected with both MN2 and MN3 (Fig. 3). In sALS, activated MG/Mϕ1 expressing MHC class I and II correlated with MN2; activated MG/Mϕ2 expressing MHC class II correlated with MN3 (Fig. 2). In sALS patients, MN3 negatively correlated with the disease course (Fig. 1C). Expressions of MHC class I and II on glial cells associated with different subtypes of MNs imply immune responses that may involve neuroinflammation and neurodegeneration in sALS. Therefore, the classification of specific cellular compositions

Table 2
Affected biological processes and gene pathways.

Patient	Cell Type	Pathway	p-value	Biological Process	p-value
Control (n = 10)	MN1	Oxytocin receptor mediated signaling	< 0.001	Heart development	< 0.01
		5HT2 type receptor mediated signaling	< 0.001	Muscle organ	< 0.05
		Alzheimer's disease-amyloid secretase	< 0.001	development	< 0.05
		Apoptosis signaling	< 0.01	Cytoskeleton organization	
		Alpha adrenergic receptor signaling	< 0.05		
		Histamine H1 receptor mediated signaling	< 0.05		
		Beta1 and Beta2 adrenergic receptor signaling	< 0.05		
	MN2	Dopamine receptor mediated signaling	< 0.05	Polyphosphate catabolic process	< 0.01
				Apoptotic process	< 0.001
				Regulation of molecular function	< 0.05
				Intracellular signal transduction	< 0.05
				Catabolic process	< 0.05
	Astrocyte	Cadherin signaling	< 0.0001	Negative regulation of	< 0.001
		Integrin signaling	< 0.0001	apoptotic process	
		Wnt signaling	< 0.001	Cell adhesion	< 0.00001
		T cell activation	< 0.01	Cellular component morphogenesis	< 0.0001
		Dopamine receptor mediated signaling	< 0.05		
		Metabotropic glutamate receptor group III	< 0.05		
		Alzheimer's disease-presenilin	< 0.05		
		Opioid prodynorphin	< 0.05		
		Opioid proopiomelanocortin	< 0.05		
		Opioid proenkephalin	< 0.05		
		FAS signaling	< 0.05		
		Serine glycine biosynthesis	< 0.05		
ALS (n = 12)	MN2	Muscarinic acetylcholine receptor 1&3 signaling	< 0.001	Cellular component movement	< 0.01
		Ionotropic glutamate receptor	< 0.001	Nervous system development	< 0.01
		Huntington disease	< 0.001	Chromosome segregation	< 0.01
		Metabotropic glutamate receptor group III	< 0.001	Cellular component morphogenesis	< 0.01
		Metabotropic glutamate receptor group I	< 0.01		
	MN3	B cell activation	< 0.0001	Calcium-mediated	< 0.01
		T cell activation	< 0.001	signaling	< 0.01
		Heterotrimeric G-protein signaling: phototransduction	< 0.001	Induction of apoptosis	< 0.01
		Heterotrimeric G-protein signaling: Gsα	< 0.01	Protein phosphorylation	
	Microglia/MΦ1	Integrin signaling	< 0.00001	Cell adhesion	< 0.00001
		FAS signaling	< 0.01	Mesoderm development	< 0.01
				Developmental process	< 0.01
	Microglia/MΦ2	T cell activation	< 0.01	Antigen processing and presentation	< 0.001
		DNA replication	< 0.01		
	Astrocyte	Parkinson's disease	< 0.05	Skeletal system development	< 0.05
		Apoptosis signaling	< 0.05	Phosphate-containing compound	< 0.01

p-values calculation by panther statistical enrichment test.

provides important tools for further developing biomarkers or therapeutic targets.

5. Discussion

Clinicopathological studies of human ALS spinal cord suggest that neurodegeneration in ALS can start focally in one region and progress to adjacent regions of the spinal cord with maximal motor neuron loss at the time of death correlating with the site of disease onset (Ravits et al., 2007a; Ravits et al., 2007b). Neuroinflammation is involved in ALS pathology in both human postmortem material and the SOD1 G93A transgenic mouse model (Beers et al., 2006) (Henkel et al., 2009) (Appel et al., 2010). It is still unclear whether or not neuroinflammation drives motor neuron death. While human studies will always be correlational, they are critically important and cannot be replaced by in vitro studies or animal models. Moreover, imaging studies in living ALS patients corroborate the findings by demonstrating increased glial activation in regions of disease onset in the brain (Zurcher et al., 2015). We are the first study to show that different subtypes of motor neurons (MN2 and MN3) connected with different groups of microglia/macrophage (MG/Mϕ1 and MG/Mϕ2) at less affected levels of spinal cord in sALS patients.

5.1. MN3 negatively associate with patient's survival and activated MG/Mϕ2 in sALS

The classification of different subtypes of motor neurons at less affected regions of spinal cord in sALS has important clinical impact. MN3 only presents in sALS patients and the higher quantity of MN3 correlates with shorter survival (Fig. 1C). While the decreased MN3 associated with increased MG/Mϕ2 (Fig. 2A), the correlation between survival and MG/Mϕ2 did not reach a significant level. Others' studies provide the evidence for the role of neuroinflammation in human ALS, such as common variants of the CX3CR1 microglial gene that influence ALS survival (Calvo et al., 2018) (Lopez-Lopez et al., 2014). TREM2 protein in *cerebrospinal fluid* (*CSF*) at late stage disease has recently been reported to predict survival in ALS (Cooper-Knock et al., 2017). We found that TREM2 in MG/Mϕ2 gene (Table 2) is upregulated but negatively associates with increased MN3 (data not shown). Although the correlation between TREM2 and survival at the less affected region showed the trend, it did not reach a significant level (data not shown). Taken together, studies from us and others support the hypothesis that the interaction and physical connection between MN3 and MG/Mϕ2 may induce bi-directional cytotoxicity of neurodegeneration and neuroinflammation and contribute to disease progression from less to more affected regions.

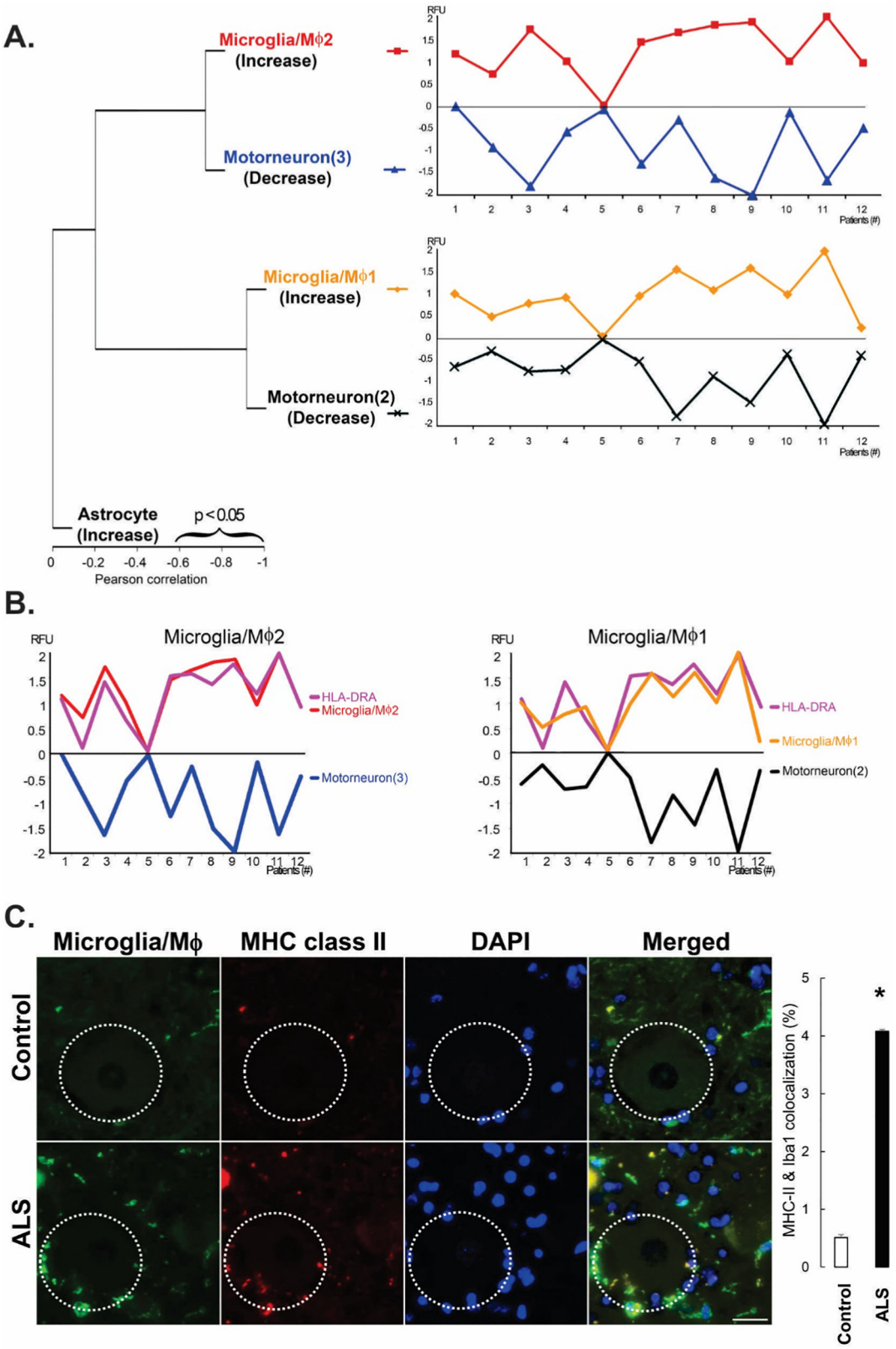

(caption on next page)

5.2. MN2 negatively associated with MG/Mϕ1 and astrocytes in sALS

Subtype 2 motor neurons (MN2) are present in both sALS and control patients (Fig. 3). Decreased MN2 associated with increased MG/Mϕ1 only presents in sALS patients (Fig. 2), suggesting that the interaction between MN2 and activated MG/Mϕ1 makes a contribution to disease progression from less to more affected levels.

Growing evidence suggests that astrocytes are involved in the survival and demise of motor neurons and a strong reactive astrogliosis surrounds degenerating motor neurons in ALS patients and ALS animal

Fig. 2. Inverse correlations between motor neurons and activated macrophage/microglia showed only in sALS patients. Analysis of the expression of DE genes crossed all the samples using "R" and Cytoscape reveals highly consistent and exact reciprocal patterns of gene clusters in sALS patients. We found profiles of decreased motor neuron genes and increased glial genes that clustered by opposite Pearson correlation. Hierarchical clustering showed an opposite and significant correlation between different subtypes of MNs (MN2 and MN3) and different subtypes of microglia/macrophages ($p < 0.05$), respectively (A). Significant correlations were between MG/Mϕ2 and MN3 ($r < -0.72, p < 0.01$); and MG/Mϕ1 and MN2 ($r < -0.91, p <$ 1E-5) (B). The expression of the HLA DRA (MHC class II) reveals a significant positive correlation with MG/Mϕ2 ($r > 0.92$, p < 1E-4) and MG/Mϕ1 ($r > 0.84$, p < 1E-3) (B). Tissue staining was performed on formalin-fixed lumbar spinal cord slides using activated microglia/macrophage specific (Iba1 = green) and MHC class II specific antibodies (HLA DRA = red) (C). Scale bar = 50 μm. Quantitation described in the Materials and Methods confirmed a significant increase in co-localization between microglia/macrophages (Iba1 = green) and MHC class II (HLA DRA = red) in sALS patients ($n = 3$) when compared to control patients (n = 3). Dotted line represents a motorneuron. *: p-value < 0.05 by student's t-test. (For interpretation of the references to colour in this figure legend, the reader is referred to the web version of this article.)

models (Ilieva et al., 2009) (Vargas and Johnson, 2010). Whether reactive astrogliosis in ALS is detrimental remains an open question; it could depend on the stage of the disease (onset vs end-stage) as well as the characteristics and environment of a particular motor neuron. A recent study showed that a subtype of reactive astrocytes (A1) is induced by classically activated neuroinflammatory microglia (Liddelow and Barres, 2017; Liddelow et al., 2017). Toxic astrocytes A1 secrete IL-1α, TNF, and C1q, and these cytokines, along with activated neuroinflammatory microglia, are necessary and sufficient to induce astrocytes A1. Astrocytes A1 lose the ability to promote neuronal survival, outgrowth, synaptogenesis, and phagocytosis, and induce the death of neurons and oligodendrocytes. Another recent study showed that astrocytes derived from sALS patients triggered necroptosis in motor neurons in a receptor-interacting protein 1-dependent manner (Re et al., 2014). Recent studies suggest that microglia and other glia promote motor neuron degeneration by inducing inflammation and necroptosis in a manner dependent on receptor-interacting kinase 1 (Ito et al., 2016) (Politi and Przedborski, 2016).

In this study, we observed that decreased MN2 associated with increased MHC class I on microglia from sALS (Fig. 4A), suggesting that other immune cells may also be involved in the process of neurodegeneration (Table 2). However, we have not found an abnormal

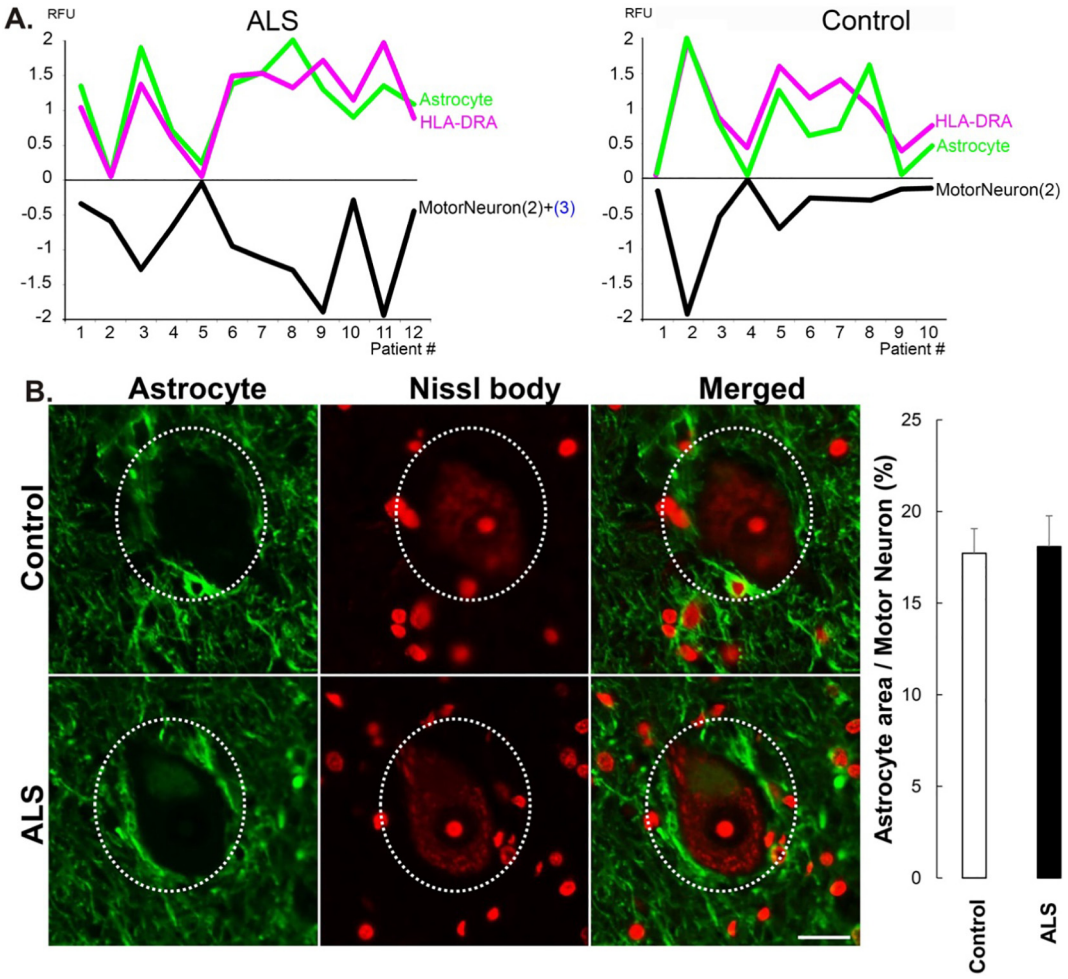

Fig. 3. Inverse correlations between motor neurons and reactive astrocytes showed in both sALS and control patients. Hierarchical clustering showed an opposite and significant correlation between motor neurons and both astrocytes and HLA-DRA (MHC class II) within the sampled area in sALS and control patients, respectively (A). Significant correlations were between MN2 + MN3 and astrocytes in 12 sALS patients ($r < -0.79, p < 0.01$); between MN2 and astrocytes (r < −0.79, p < 0.01) in 10 control patients. The expression of the HLA DRA (MHC class II) reveals a significant positive correlation with activated astrocytes ($r > 0.83$, p < 0.01). Tissue staining was performed on formalin-fixed lumbar spinal cord slides using reactive astrocyte specific antibody (GFAP = green) and Nissl body (red) for staining motor neurons (B). Scale bar = 50 μm. Quantitation described in the Materials and Methods confirmed no significant change of astrocytes within the sampled areas between sALS patients ($n = 3$) and control patients (n = 3). Dotted line represents a motorneuron. (For interpretation of the references to colour in this figure legend, the reader is referred to the web version of this article.)

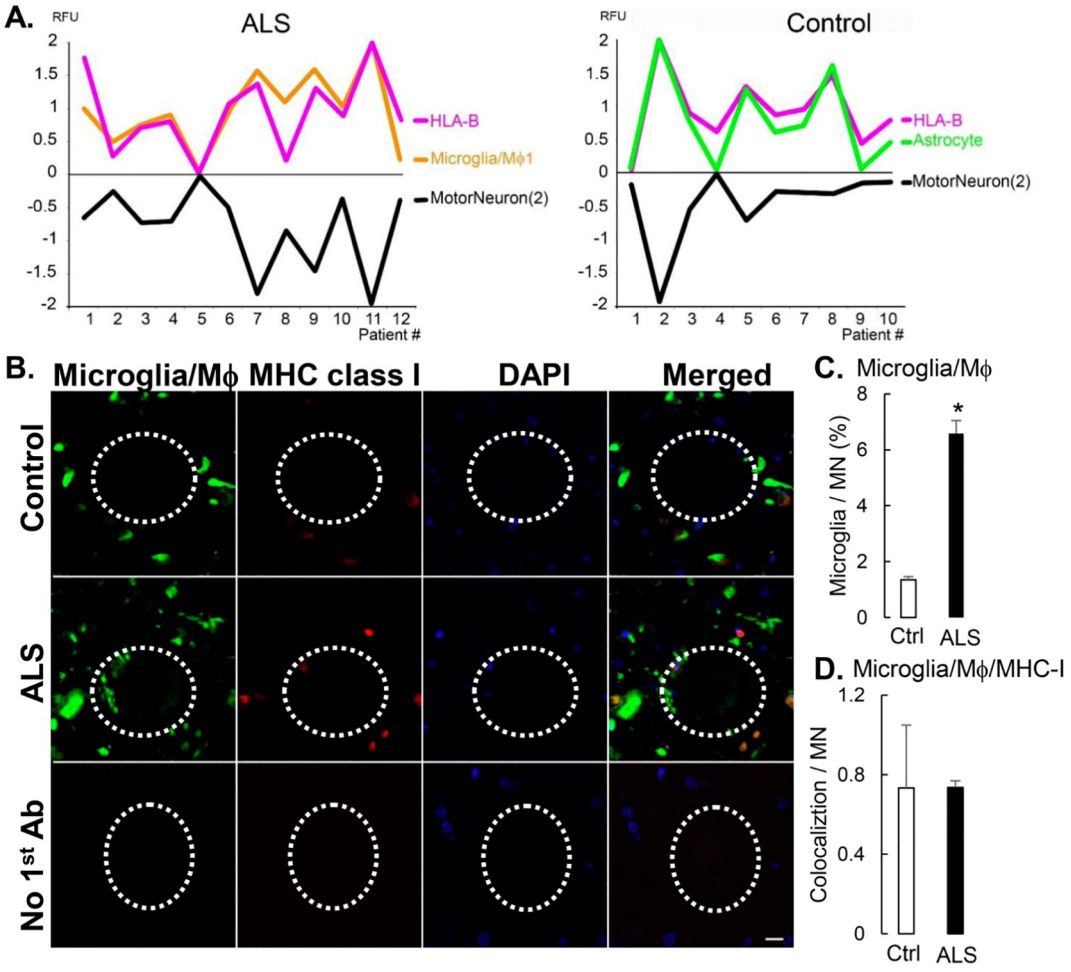

Fig. 4. Inverse correlations between motor neurons and MHC class I showed in both sALS and control patients. Hierarchical clustering showed an opposite and significant correlation between HLA-B (MHC class I) and motor neuron (MN2) within the sampled area in both sALS and control patients, respectively (A). Significant correlations were between MHC class I and MN2 in 12 sALS patients ($r < -0.80$, $p < 0.01$) and between MHC class I and MN2 in 10 control patients ($r < -0.78$, $p < 0.01$). Tissue staining was performed on formalin-fixed lumbar slides using MHC class I (HLA A/B/C = red) and activated microglia/macrophage (Iba1 = green) specific antibodies (B). Quantitation described in the Materials and Methods confirmed no significant change of MHC class I within the sampled areas between the ALS patients ($n = 3$) compared to control patients (n = 3). Dotted line represents a motorneuron. (For interpretation of the references to colour in this figure legend, the reader is referred to the web version of this article.)

reduction of HLA-F (Song et al., 2016), a MHC class I molecule, in these laser captured motor neurons from less affected regions of spinal cords.

5.3. Similarities and differences between MN2 and astrocytes in sALS vs. controls

It seems that all MN2 and astrocytes share certain common patterns of gene expression in both sALS and control patients (Figs. 1B and 5,

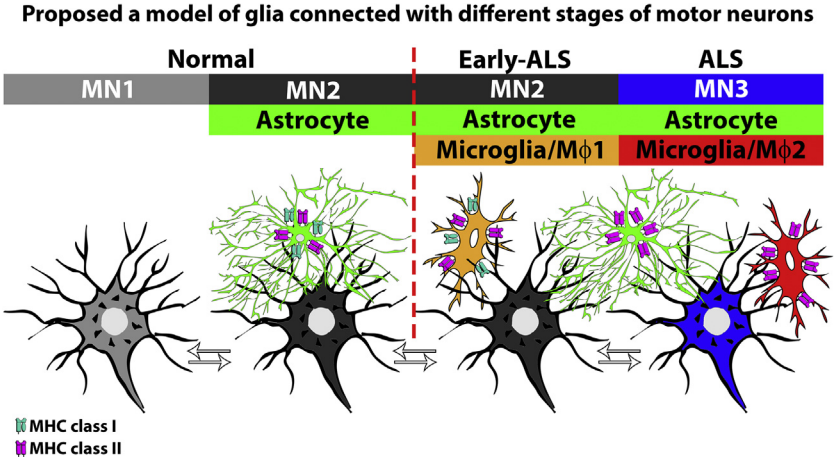

Fig. 5. Proposed a model of glia connected with different subtypes of motor neurons. MN1 and MN2 were present in control patients. MN2 and MN3 were present in sALS patients. In control patients, reactive astrocytes expressing both MHC class I and II connected with MN2. In sALS patients, reactive astrocytes expressing MHC class II connected with both MN2 and MN3. In sALS, MG/Mϕ1 expressing MHC class I and II correlated with MN2; and MG/Mϕ2 expressing MHC class II correlated with MN3. Expressions of MHC class I and II on glial cells associated with different subtypes of MNs imply immune responses that may involve neuroinflammation and neurodegeneration in sALS. The schematic diagram presents a proposed and simplified model of activated glia that connects different subtypes of motor neurons in control and sALS patients suggesting that the specific cellular compositions in sALS could be biomarkers or therapeutic targets. Signaling within and between subtypes of motor neurons and glia could both contribute to disease progression.

Table 1). However, the biological processes and gene pathways differ between MN2 in controls vs. MN2 in ALS and astrocytes in controls sv. astrocytes in ALS (Table 2). We noted that other cell subtypes also connected to MN2 besides astrocytes in sALS. In sALS patients, MN2 connected not only with astrocytes but also with microglia/Mϕ1 (Figs. 2A, B, 3A and 5). Astrocytes connected not only with MN2 but also with MN3 (Figs. 3A and 5) in sALS patients. Additional connections of MN2 and astrocytes with other cell subtypes in sALS patients likely affect the biological processes and gene pathways differently compared to control patients.

In summary, we identified that distressed motor neurons (MN2 and NM3) were closely surrounded by activated microglia/macrophage (MG/Mϕ1 and MG/Mϕ2) in the less affected regions of the spinal cord in sALS patients. While the exact mechanism of how activated microglia/macrophages promotes neurodegenerative progression is unclear, the findings support the hypothesis that neuro-glia physical interactions are important in pathogenesis, and targeting disease-specific motor neurons and/or glia could be a useful therapy to slow disease progression.

Acknowledgements

This work was supported in part by the startup fund from the department of Neurology and Rehabilitation, University of Illinois at Chicago (to F.S.). We thank Ms. Sarah Martin for editing the manuscript.

Author contributions

F.D. and J.L. conducted experiments and analyzed the data. F.S. planned the study. F.D., J.R. and F.S. wrote the manuscript.

Competing interests

The authors declare no competing both financial and non-financial interests.

Appendix A. Supplementary data

Supplementary data to this article can be found online at https://doi.org/10.1016/j.nbd.2019.104523.

References

Appel, S.H., 2009. CD4+ T cells mediate cytotoxicity in neurodegenerative diseases. J. Clin. Investig. 119.
Appel, S.H., et al., 2010. T cell-microglial dialogue in Parkinson's disease and amyotrophic lateral sclerosis: are we listening? Trends Immunol. 31 SRC - BaiduScholar 7–17.
Beers, D.R., et al., 2006. Appel microglia extend survival in PU. 1 knockout mice with familial amyotrophic lateral sclerosis. In: Proceedings of the National Academy of Sciences of the United States of America. 103 SRC - BaiduScholar, pp. 16021–16026.
Beers, D.R., et al., 2008. CD4+ T cells support glial neuroprotection, slow disease progression, and modify glial morphology in an animal model of inherited ALS. Proc. Natl. Acad. 105 SRC - BaiduScholar 15558–15563.
Boillee, S., et al., 2006. ALS: a disease of motor neurons and their nonneuronal neighbors. Neuron. 52, 39–59.
Byrne, S., et al., 2011. Rate of familial amyotrophic lateral sclerosis: a systematic review and meta-analysis. J. Neurol. Neurosurg. Psychiatry 82, 623–627.
Calvo, A., et al., 2018. Chiò a. common polymorphisms of chemokine (C-X3-C motif) receptor 1 gene modify amyotrophic lateral sclerosis outcome: a population-based study. Muscle. Nerve. Feb. 57, 212–216.
Cooper-Knock, J., et al., 2017. A data-driven approach links microglia to pathology and prognosis in amyotrophic lateral sclerosis. Acta Neuropathol. Commun. 5, 23.
Dachet, F., et al., 2015. Predicting novel histopathological microlesions in human epileptic brain through transcriptional clustering. Brain 138, 356–370.
Frakes, A.E., et al., 2014. Microglia induce motor neuron death via the classical NF-kappaB pathway in amyotrophic lateral sclerosis. Neuron 81, 1009–1023.
Graber, D.J., et al., 2010. Progressive changes in microglia and macrophages in spinal cord and peripheral nerve in the transgenic rat model of amyotrophic lateral sclerosis. J. Neuroinflammation 7, 8.
Henkel, J.S., et al., 2009. Microglia in ALS: the good, the bad, and the resting. J. NeuroImmune Pharmacol. 4, 389–398.
Ilieva, H., et al., 2009. Non-cell autonomous toxicity in neurodegenerative disorders: ALS and beyond. Biol 187, 761–772.
Ito, Y., et al., 2016. RIPK1 mediates axonal degeneration by promoting inflammation and Necroptosis in ALS. Science. 353, 603–608.
Kawamata, T., et al., 1992. Immunologic reactions in amyotrophic lateral sclerosis brain and spinal cord tissue. Am. J. Pathol. 140, 691–707.
Liddelow, S.A., Barres, B.A., 2017. Reactive astrocytes: production, function, and therapeutic potential. Immunity 46, 957–967.
Liddelow, S.A., et al., 2017. Neurotoxic reactive astrocytes are induced by activated microglia. Nature 541.
Lopez-Lopez, A., et al., 2014. Rodríguez MJ, CX3CR1 Is a Modifying Gene of Survival and Progression in Amyotrophic Lateral Sclerosis. PLo May 7e96528. pp. 9.
McGeer, P.L., et al., 1993. Microglia in degenerative neurological disease. Glia. Jan Review. 7, 84–92.
Nardo, G., et al., 2016. Major histocompatibility complex I expression by motor neurons and its implication in amyotrophic lateral sclerosis. Front. Neurol. 7, 89.
Perry, V.H., et al., 2010. Microglia in neurodegenerative disease. Nat. Rev. Neurol. 6.
Politi, K., Przedborski, S., 2016. Axonal degeneration: RIPK1 multitasking in ALS. Curr. Biol. Cb. 26.
Rabin, S.J., et al., 2010. Has compartment-specific aberrant exon splicing and altered cell-matrix adhesion biology. Hum. Mol. Genet. 19, 313–328.
Ravits, J.M., Spada, A.R.L., 2009. ALS motor phenotype heterogeneity, focality, and spread deconstructing motor neuron degeneration. Neurology 73, 805–811.
Ravits, J., et al., 2007a. Implications of ALS focality: rostral-caudal distribution of lower motor neuron loss postmortem. Neurology 68, 1576–1582.
Ravits, J., et al., 2007b. Jorg of upper and lower motor neuron degeneration at the clinical onset of ALS. Neurology 68, 1571–1575.
Re, D.B., et al., 2014. Le Necroptosis drives motor neuron death in models of both sporadic and familial ALS. Neuron 81, 1001–1008 Mar 5.
Rowland, L.P., Shneider, N.A., 2001. Amyotrophic lateral sclerosis. N. Engl. J. Med. 344, 1688–1700.
Sargsyan, S.A., et al., 2005. Microglia as potential contributors to motor neuron injury in amyotrophic lateral sclerosis. Glia 51, 241–253.
Smoot, M.E., et al., 2011. Cytoscape 2.8: new features for data integration and network visualization. Bioinformatics 27, 431–432.
Song, F., et al., 2012. Aberrant neuregulin 1 signaling in amyotrophic lateral sclerosis. J. Neuropathol. Exp. Neurol. 71, 104–115.
Song, F., et al., 2014. Activation of microglial neuregulin1 signaling in the corticospinal tracts of ALS patients with upper motor neuron signs. Amyotroph. Lateral Scler. Frontotemporal Degener. 15, 77–83.
Song, S., et al., 2016. Major histocompatibility complex class I molecules protect motor neurons from astrocyte-induced toxicity in amyotrophic lateral sclerosis. Nat. Med. 22, 397–403.
Turner, M.R., et al., 2004. Evidence of widespread cerebral microglial activation in amyotrophic lateral sclerosis: an [11C](R)-PK11195 positron emission tomography study. Neurobiol. Dis. 15, 601–609.
Vargas, M.R., Johnson, J.A., 2010. Astrogliosis in amyotrophic lateral sclerosis: role and therapeutic potential of astrocytes. Neurotherapeutics 7, 471–481.
Yamanaka, K., et al., 2008. Astrocytes as determinants of disease progression in inherited ALS. Nat. Neurosci. 11, 251–253.
Zurcher, N.R., et al., 2015. Increased in vivo glial activation in patients with amyotrophic lateral sclerosis: assessed with [(11)C]-PBR28. Neuroimage Clin 7, 409–414.